Mean-square radii of two-component three-body systems in two spatial dimensions

J. H. Sandoval,[1] F. F. Bellotti,[2] A. S. Jensen,[2] and M. T. Yamashita[1]
[1]*Instituto de Física Teórica, UNESP - Univ Estadual Paulista, C.P. 70532-2, CEP 01156-970, São Paulo, SP, Brazil*
[2]*Department of Physics and Astronomy, Aarhus University, DK-8000 Aarhus C, Denmark*
(Received 5 April 2016; revised manuscript received 16 May 2016; published 31 August 2016)

We calculate root-mean-square radii for a three-body system confined to two spatial dimensions and consisting of two identical bosons (A) and one distinguishable particle (B). We use zero-range two-body interactions between each of the pairs, and focus thereby directly on universal properties. We solve the Faddeev equations in momentum space and express the mean-square radii in terms of first-order derivatives of the Fourier transforms of densities. The strengths of the interactions are adjusted for each set of masses to produce equal two-body bound-state energies between different pairs. The mass ratio, $\mathcal{A} = m_B/m_A$, between particles B and A are varied from 0.01 to 100, providing a number of bound states decreasing from 8 to 2. Energies and mean-square radii of these states are analyzed for small $\mathcal{A}$ by use of the Born-Oppenheimer potential between the two heavy A particles. For large $\mathcal{A}$ the radii of the two bound states are consistent with a slightly asymmetric three-body structure. When $\mathcal{A}$ approaches thresholds for binding of the three-body excited states, the corresponding mean-square radii diverge inversely proportional to the deviation of the three-body energy from the two-body thresholds. The structures at these three-body thresholds correspond to bound AB dimers and one loosely bound A particle.

DOI: 10.1103/PhysRevA.94.022514

I. INTRODUCTION

The last decade has provided unprecedented accurate techniques to tune the effective interactions between pairs of ultracold atoms in extremely controllable external fields. The effective two-body interactions can be varied, for a number of special atoms, from strongly attractive to strongly repulsive by use of the Feshbach resonance technique; see review in Ref. [1]. The two-body interactions are experimentally determined functions of the applied magnetic field strength. The atomic gases, possibly with different atoms, are confined by flexible deformed external fields. Ultimately this allows extreme asymmetry corresponding to spatial dimensions lower than three [2,3]. Structures of different systems can then be simulated and studied.

Our interests in the present investigation are three-body structures and two-dimensional universal properties. First, few-body physics is by definition accurately solvable without approximations in contrast to many-body physics. But now experimental tests can be made for many of the claims derived by theoretical calculations. We focus here on the absolutely simplest unsolved system of three particles in two spatial dimensions (2D). Second, the physics in 2D differ enormously from the much more known properties in three dimensions (3D) and for that matter any other spatial dimension [4,5]. Third, the many universal properties are arguably the most important results confirmed by cold atomic gas experiments. Properly formulated they are applicable throughout physics as independent of scale and details of the corresponding potentials [6,7].

The third of these points refer to the concept of universality which means that the related properties can be described by only a few scale parameters [8]. The interactions between neutral atoms in dilute atomic gases are of very short range compared to the two-body scattering length [9–11]. This implies that low-energy observables are universal and only depend on the scattering length which can be the same for disparate potentials. Thus the universal regime can be defined as properties depending only on lengths far larger than the range of the potential and far smaller than the scattering length. Thus, a zero-range interaction with its strength proportional to the scattering length is automatically focussing on universal properties.

The special interest in two dimensions is due to the properties arising from the negative centrifugal barrier corresponding to the relative coordinate between two particles. This means that binding is achieved even with an infinitesimal attraction between the two particles. Also three particles are bound in 2D with almost vanishing attractive two-body potentials. For identical bosons in the universal regime all observables in 2D can be expressed as functions of only one two-body scale parameter, e.g., the two-body scattering length [6,7]. In 3D, both a two- and a three-body scale parameter are needed to describe universal observables [12]. This difference is closely related to the appearance of the pathological Efimov effect for three particles in 3D [13] and its absence in 2D [14]. This apparent discontinuity can now be studied with external traps varying continuously from spherical to cylindrical geometry [15].

The status for weakly bound three-body systems in 2D is that energies are well studied theoretically [16–26]. The simplest reference system we have is three identical bosons with only two three-body bound states with energies E_3 proportional to the two-body energy E_2, that is, $E_3 = 16.52E_2$ and $E_3 = 1.27E_2$ [16]. The previous studies include energies of three nonidentical particles where different masses and scattering lengths substantially complicate systematic characterization of the universal properties [19]. The simplest asymmetric system, denoted AAB, is formed by two identical bosons A and a distinguishable particle B. With spin-independent interactions, the results also apply to two identical fermions with symmetric spatial wave function. The number of three-body bound states increases as the mass ratio $\mathcal{A} = m_B/m_A$ between B and A decreases [21]. Then the B particle can be exchanged more easily between the heavy A particles, which in turn generates an effective

potential eventually of infinite attraction for vanishing $\mathcal{A}$ [22,24,27].

In contrast to the energies, knowledge about structures of asymmetric three-body systems in 2D is virtually not existing. One reason is that experiments have only now become feasible, but the lack of the necessary operating theoretical techniques is probably also partly responsible for this delay. Most of the studies have employed zero-range interactions treated in momentum space, and have calculated energies without direct access to the corresponding wave functions. The structures therefore require a substantially larger additional effort. Coordinate space calculations in 2D with direct links to wave functions are also not available at the moment.

We shall continue to use the zero-range interaction with the easy interpretation in terms of universal properties [28]. It is worth mentioning that it would be interesting to extend the present calculation to more than three atoms to see how the universal relations derived in [29] would change for a mass-imbalanced situation. We use tedious mathematics to express various radial moments of relative distances as derivatives of momentum-space integrals. This is instead of the extensive numerical computation of momentum-space wave functions with subsequent Fourier transformation and derivation of structural properties. We shall be content with second radial moments, which are the simplest observable quantities that carry structure information. If necessary, higher moments can also be computed by use of the same technique, but we believe the second radial moments of various relative distances are sufficient to extract the dominating underlying structure.

The paper is organized as follows. In Sec. II we give first the appropriate Faddeev equations in momentum space for an AAB system of one distinguishable and two identical particles. Then we construct the three-body wave functions and the form factors from which the radii of interest are calculated. In Sec. III we present and analyze numerical results of energy spectra and mean-square radii, as functions of the mass ratio. In particular, we discuss the threshold behavior when a level is passing into the three-body continuum of one particle and a bound pair. Finally, conclusions and perspectives are summarized in Sec. IV.

II. THEORETICAL FORMULATION

We consider a three-body system, AAB, consisting of two identical bosons A of mass m_A and bound-state energy $E_{AA} < 0$, and a third distinguishable particle B of mass m_B bound to each A particle with energy $E_{AB} < 0$. We denote the identical particles by A and A' when it is necessary to distinguish their coordinates. The two-body interactions are assumed to be of very short range, and in this paper they are parametrized and applied in the extreme zero-range limit where only s waves are important. This rather schematic interaction extracts universal properties due to the absence of spatial regions inside the potential.

A. Faddeev equations

The preferred method in most investigations is the use of the Faddeev decomposition in momentum space. The theoretical formulation is a little elaborate but available in detail in the literature [7,8]. We shall here only specify our notation and present the Faddeev equations in momentum space. We shall then proceed to sketch the derivation of the different mean-square radii expressed as derivatives of integrals over the momentum-space solutions. The three-body state $|\Psi_{AAB}\rangle$ corresponds to the three-body momentum-space wave function $\Psi_{A'B,A}$ when it is expressed in terms of $\vec{p}_A$ and $\vec{q}_A$, that are, respectively, the relative momenta between the B and the A' particle, and the center of mass of $A' + B$ and the A particle. The Faddeev decomposition then amounts to

$$\begin{aligned}\Psi_{AB,A}(\vec{q}_A,\vec{p}_A) &\equiv \langle \vec{q}_A,\vec{p}_A\,|\Psi_{AAB}\rangle \\ &= \frac{\chi_A(|\vec{q}_A|)+\chi_B\left(|\vec{p}_A-\frac{\mathcal{A}}{\mathcal{A}+1}\vec{q}_A|\right)+\chi_A\left(|\vec{p}_A+\frac{1}{\mathcal{A}+1}\vec{q}_A|\right)}{|E_3|+\frac{\mathcal{A}+1}{2\mathcal{A}}\frac{p_A^2}{m_A}+\frac{\mathcal{A}+2}{2(\mathcal{A}+1)}\frac{q_A^2}{m_A}},\end{aligned} \tag{1}$$

where $|E_3|$ is the three-body binding energy, the mass ratio between particles B and A is denoted $\mathcal{A} \equiv m_B/m_A$, and the so-called spectator functions, the Faddeev components χ_A and χ_B, are given as functions of the relative momenta in the corresponding Jacobi coordinates, that are, $\vec{q}_A$, $\vec{q}_B$, and $\vec{q}_{A'}$, where

$$\vec{q}_B = \vec{p}_A - \frac{\mathcal{A}}{\mathcal{A}+1}\vec{q}_A, \quad \vec{q}_{A'} = \vec{p}_A + \frac{1}{\mathcal{A}+1}\vec{q}_A. \tag{2}$$

The spectator functions χ_A and χ_B obey coupled integral equations obtained after s-wave projection. The detailed standard derivation of these equations in 2D can be found in [20], with the result

$$\begin{aligned}\chi_B(q) &= 2\tau_{AA}\left(|E_3|+\frac{\mathcal{A}+2}{4\mathcal{A}}\frac{q^2}{m_A}\right) \\ &\quad\times\int d^2p\,G_1(p,q;E_3)\chi_A(p)\end{aligned} \tag{3}$$

$$\begin{aligned}\chi_A(q) &= \tau_{AB}\left(|E_3|+\frac{\mathcal{A}+2}{2(\mathcal{A}+1)}\frac{q^2}{m_A}\right) \\ &\quad\times\int d^2p[G_1(q,p;E_3)\chi_B(p)+G_2(q,p;E_3)\chi_A(p)].\end{aligned} \tag{4}$$

$$G_1(q,p;E_3) = \frac{1}{|E_3|+\frac{q^2}{m_A}+\frac{\mathcal{A}+1}{2\mathcal{A}}\frac{p^2}{m_A}+\frac{\vec{q}\cdot\vec{p}}{m_A}}, \tag{5}$$

$$G_2(q,p;E_3) = \frac{1}{|E_3|+\frac{\mathcal{A}+1}{2\mathcal{A}}\frac{(q^2+p^2)}{m_A}+\frac{1}{\mathcal{A}}\frac{\vec{q}\cdot\vec{p}}{m_A}}, \tag{6}$$

where the two-body T matrices $\tau_{A\alpha}$ of the interacting pair are given by

$$\tau_{A\alpha}(E) = \left[-4\pi\frac{m_A m_\alpha}{m_A+m_\alpha}\ln\left(\sqrt{\frac{|E|}{|E_{A\alpha}|}}\right)\right]^{-1}, \tag{7}$$

where $E_{A\alpha}$ is the two-body binding energy of the pair $A\alpha$, with $\alpha = A,B$.

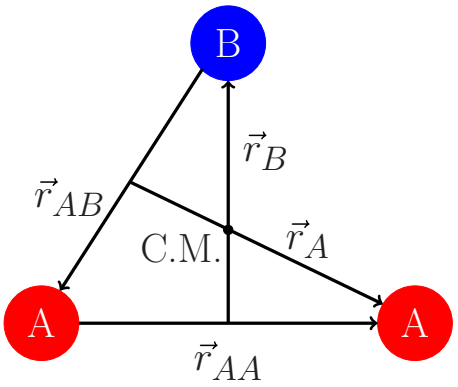

FIG. 1. Schematic figure showing the three-body system of two identical bosons A and one distinguishable particle B. The vectors $\vec{r}_{AB}$ and $\vec{r}_{AA}$ are relative distances between the respective pairs of particles, whereas $\vec{r}_A$ and $\vec{r}_B$ denote distances between the specified particle and the center of mass of the remaining pairs. The point marked C.M. means center of mass of the three-body system. The notation used in the paper for the relevant distances is also shown.

B. Mean-square radii

The distances in the three-body system can be seen in Fig. 1, where $\vec{r}_{AB}$, $\vec{r}_{AA'}$, and $\vec{r}_{A'B}$, are relative distances between pairs of particles, and $\vec{r}_{A'}$, $\vec{r}_{A'}$, and $\vec{r}_B$ denote distances between the center of mass of such pairs and the remaining last particle. The momenta $\vec{q}_A$ and $\vec{p}_A$ are, respectively, canonically conjugated to the radii $\vec{r}_A$ and $\vec{r}_{AB}$.

The mean-square radii can be computed from the momentum-space wave function by Fourier transform and subsequent calculation of the corresponding matrix element. To be precise we first define one-body densities related to one set of Jacobi coordinates, $\vec{r}_A$ and $\vec{r}_{AB}$, that is,

$$\rho(\vec{r}_A) = \int d^2 r_{AB} |\langle \vec{r}_A, \vec{r}_{AB} | \Psi_{AAB} \rangle|^2, \tag{8}$$

$$\bar{\rho}(\vec{r}_{AB}) = \int d^2 r_A |\langle \vec{r}_A, \vec{r}_{AB} | \Psi_{AAB} \rangle|^2, \tag{9}$$

where $\langle \vec{r}_A, \vec{r}_{AB} | \Psi_{AAB} \rangle$ is the coordinate-space wave function expressed in terms of $\vec{r}_A$ and $\vec{r}_{AB}$. We first expand the Fourier transform F_A of $\rho(\vec{r}_A)$ to second order in the corresponding momentum, that is,

$$F_A(Q^2) = \int d^2 r_A e^{\frac{i}{\hbar}\vec{Q}\cdot\vec{r}_A} \rho(r_A) \approx 1 - \frac{1}{4\hbar^2} Q^2 \langle r_A^2 \rangle, \tag{10}$$

$$\langle r_A^2 \rangle = \int d^2 r_A r_A^2 \rho(r_A), \tag{11}$$

where we assumed a normalized one-body density and used that all odd powers of $\vec{Q}$ vanish due to spherical symmetry. The first-order derivative with respect to Q^2 then gives the desired mean-square radius. In the same way we obtain

$$\langle r_{AB}^2 \rangle = \int d^2 r_{AB} r_{AB}^2 \bar{\rho}(r_{AB}) \tag{12}$$

from the Fourier transform $F_{AB}(Q^2)$ of $\bar{\rho}(\vec{r}_{AB})$. These Fourier transforms are related to the momentum-space wave function in Eq. (1) by

$$F_A(Q^2) = \int d^2 q d^2 p \Psi_{AB,A}\left(\vec{q} + \frac{\vec{Q}}{2}, \vec{p}\right) \Psi_{AB,A}\left(\vec{q} - \frac{\vec{Q}}{2}, \vec{p}\right), \tag{13}$$

$$F_{AB}(Q^2) = \int d^2 q d^2 p \Psi_{AB,A}\left(\vec{q}, \vec{p} + \frac{\vec{Q}}{2}\right) \Psi_{AB,A}\left(\vec{q}, \vec{p} - \frac{\vec{Q}}{2}\right), \tag{14}$$

which can be verified by directly inserting the definitions of $\rho(r_A)$ and $\rho(r_{AB})$ from Eqs. (8) and (9) into Eq. (10) and the corresponding definition of $F_{AB}(Q^2)$.

To calculate the remaining mean-square radii we express the three-body wave function in the set of Jacobi momenta of the B particle, $\Psi_{AA,B}(\vec{q}_B, \vec{p}_B) \equiv \langle \vec{q}_B, \vec{p}_B | \Psi \rangle$. The mean-square radii $\langle r_B^2 \rangle$ and $\langle r_{AA}^2 \rangle$ are then obtained as first-order derivatives with respect to Q^2 of the Fourier transforms, $F_B(Q^2)$ and $F_{AA}(Q^2)$, defined by replacing $\Psi_{AB,A}$ with $\Psi_{AA,B}$ in Eqs. (13) and (14).

The procedure is now to solve the three-body equations in Eqs. (3) and (4) and obtain three-body energy, spectator functions, and the total wave function in Eq. (1). The next steps are to calculate numerically F_A, F_B, F_{AA}, and F_{AB} and the necessary first-order derivatives of these functions of the squared momenta.

III. MASS DEPENDENCE

The three-body wave function is completely determined from the two ratios of particle masses, $\mathcal{A} = m_B/m_A$, and two-body bound-state energies, E_{AA}/E_{AB}, both negative. To extract meaningful structure properties it is crucial to know all independent distances in a given system, as illustrated in Fig. 1. We calculate energies and radii of the lowest-lying excited states as functions of $\mathcal{A}$ for an energy ratio of $E_{AA}/E_{AB} = 1$. Each of the two-body energies results from the related reduced mass, which therefore is varied in our investigations. The calculated results therefore illustrate typical behavior of mean-square radii and structure in general. We confirm this expectation with test calculations of varying energy ratio.

A. Three-body energies

The energy is for most quantum states the all-important characterizing quantity which is necessary to understand first. Universal structure of weakly bound systems often relates spatial extension and binding energy [19]. We therefore first focus on the energy dependence of the system AAB, sketched in Fig. 1. We solve the coupled set of integral equations, Eqs. (3) and (4), and show the calculated energy spectrum in Fig. 2. For $\mathcal{A} = 1$ we recover the well-known results that only ground and first excited states are bound with universally given energies, $E_3 = 16.52 E_{AB}$ and $E_3 = 1.27 E_{AB}$. These energies are predicted by a number of entirely different calculations [16,19,21].

Upon increasing the mass ratio above unity, $\mathcal{A} \geqslant 1$, the two bound states remain with moderate relative energy variations. This may be understood from the limit of one very heavy particle surrounded by two light masses moving around the

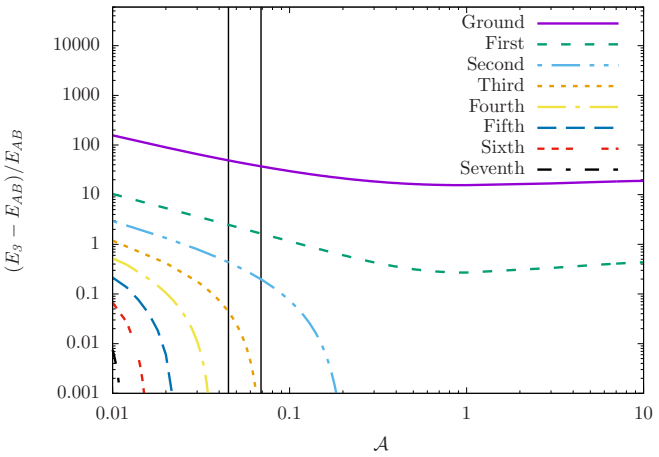

FIG. 2. Low-energy spectrum of an AAB system as a function of the mass ratio $\mathcal{A} = m_B/m_A$. The two two-body energies are equal, $E_{AB} = E_{AA}$, and the three-body energy is E_3. The energies on the y axis are given relative to the two-body bound-state energies E_{AB}. The vertical lines indicate the mass ratios $\mathcal{A} = 6/133$ and $\mathcal{A} = 6/87$ corresponding to the systems ^{6}Li-^{133}Cs-^{133}Cs and ^{6}Li-^{87}Rb-^{87}Rb.

center of mass in a roughly mass-independent field. Superficially this resembles a helium atom with two electrons moving around the four bound nucleons. However, the interactions differ enormously from the long-range Coulomb potential to the zero-range interaction. The properties in 2D also differ enormously from the 3D calculations of a helium atom. These differences are evident from the order-of-magnitude-larger ground-state binding of three particles compared to two particles.

In the other limit of small $\mathcal{A}$ we find a tremendous increase of bound states with decreasing mass ratio $\mathcal{A}$. The smallest mass ratio we consider is $\mathcal{A} = 0.01$, where the system displays eight bound states. The excited three-body states disappear into the continuum of positive energies as $\mathcal{A}$ increases from very small values. The rather dramatic mass dependence for small $\mathcal{A}$ can be understood as a consequence of the increase of the effective interaction generated by the light particle. This has been known since 1979 [30] and 1980 [27] for systems in three and two dimensions, respectively.

Recently, a different technique was used to derive an effective two-body potential in two dimensions [22]. This derivation assumed the Born-Oppenheimer approximation whose validity only is justified for $\mathcal{A} \ll 1$. After integrating out the coordinate of particle B, an effective Hamiltonian is left for the relative motion of the two heavy A particles, that is,

$$H_{\rm BO} = -\frac{\hbar^2}{2\mu_{AA}}\Delta_{\vec{r}_{AA}} + V_{AA}(r_{AA}) + V^{\rm (BO)}(r_{AA}), \qquad (15)$$

where $\vec{r}_{AA}$ is the relative coordinate between the two A particles, μ_{AA} and $V_{AA}(r)$ are their reduced mass and two-body potential, and $V^{\rm (BO)}(r_{AA})$ is the strongly $\mathcal{A}$-depending Born-Oppenheimer potential resulting from the light third particle B.

The Born-Oppenheimer potential is obtained by standard derivation in three-body physics, that is, with two centers at a fixed distance interacting with the light particle through zero-range interactions. This quantum mechanical problem in 2D is solved in the center of mass of the total system. The result is in Ref. [22] found to be

$$\ln\frac{|V^{\rm (BO)}(R)|}{|E_{AB}|} = 2K_0\left(\sqrt{\frac{2\mu_{AA,B}|V^{\rm (BO)}(R)|}{\hbar^2}}r_{AA}\right), \qquad (16)$$

where K_0 is a Bessel function, $\mu_{AA,B}$ is the reduced mass of B versus the AA system, and $R = r_{AA}\sqrt{m_A|E_{AB}|/\hbar^2}$ with $\mu_{AA,B}$. This analytical result was in Ref. [22] shown to be well approximated as a function of $\mathcal{A} = m_B/m_A$ by simpler expressions in both limits of small and large distances. The $\mathcal{A}$ dependence is through the combination

$$m_{\rm eff} = \left(\frac{4\mathcal{A}}{2+\mathcal{A}}\right)^{1/2}, \qquad (17)$$

and the results from Ref. [22] are

$$V^{\rm (BO)}(r_{AA}) \approx -\frac{2|E_{AB}|\exp(-\gamma)}{Rm_{\rm eff}} \qquad (18)$$

for $Rm_{\rm eff} \leqslant 1.15$, where $\gamma = 0.5772156649$ is Euler's constant, and

$$V^{\rm (BO)}(r_{AA}) \approx -|E_{AB}|\left(1 + \frac{\sqrt{2\pi}\exp(-Rm_{\rm eff})}{\sqrt{Rm_{\rm eff}}}\right) \qquad (19)$$

for $Rm_{\rm eff} \geqslant 1.15$. These approximations are accurate to better than 10%, where the largest deviations found around $Rm_{\rm eff} = 1.15$ [22].

The short-distance part exhibits an attractive Coulombic behavior in Eq. (18). The large-distance behavior in Eq. (19) is exponentially convergent toward the negative two-body energy E_{AB}, with a length scale proportional to $1/m_{\rm eff}$. Thus, only a finite number of bound states below E_{AB} are possible, although that number would increase without limit since the $1/m_{\rm eff}$ diverges with vanishing mass ratio $\mathcal{A}$. However, we are mostly interested in the lowest energy states which necessarily are located in the strongly attractive region at smaller distances. The small-distance Coulomb-like behavior is controlled by an effective charge squared $Z^2_{\rm eff}$ defined by

$$Z^2_{\rm eff} = \frac{2\hbar\exp(-\gamma)\sqrt{|E_{AB}|}}{m_{\rm eff}\sqrt{m_A}}. \qquad (20)$$

The kinetic energy operator in Eq. (15) has a mass of $\mu_{AA} = m_A/2$, and in two dimensions the crucial negative centrifugal barrier term corresponds to the angular-momentum quantum number of $\ell = -1/2$. The Coulomb energy spectrum for this small-distance behavior is therefore

$$\begin{aligned} E_3^{\rm (BO)} &= -\frac{Z^4_{\rm eff}\mu_{AA}}{2\hbar^2}\frac{1}{(n_r+\ell+1)^2} \\ &= \frac{(1+\mathcal{A}/2)}{2\mathcal{A}}\frac{\exp(-2\gamma)|E_{AB}|}{(n_r+\ell+1)^2} \\ &= \frac{0.630473504(1+\mathcal{A}/2)|E_{AB}|}{\mathcal{A}(2n_r+1)^2}. \end{aligned} \qquad (21)$$

The entire Coulomb spectrum is then obtained with $n_r = 0,1,2,\ldots$ and $\ell = -1/2,1/2,3/2,5/2\ldots$

TABLE I. Energies of ground and first excited states for the mass ratios $\mathcal{A} = 0.01,\ 0.02$ for the analytic Born-Oppenheimer approximation, $E_3^{(\mathrm{BO})}/E_{AB}$ [in Eq. (21)], the numerical results both without, $E_3^{(\mathrm{NI})}/E_{AB}$, and with, E_3/E_{AB}, interaction between the two heavy A particles.

State	$\mathcal{A}$	$E_3^{(\mathrm{BO})}/E_{AB}$	$E_3^{(\mathrm{NI})}/E_{AB}$	E_3/E_{AB}
Ground	0.01	63.04	53.07	157.56
	0.02	31.52	27.76	90.75
First	0.01	7.00	7.72	11.34
	0.02	3.50	4.25	6.36
Second	0.01	2.52	3.21	3.94
	0.02	1.26	1.92	2.34
Third	0.01	1.28	1.92	2.18
	0.02	0.64	1.28	1.42

We can use Eq. (21) as a useful reference spectrum for comparison to the energies in the limit of $\mathcal{A} \ll 1$, shown in Fig. 2. To do this we have to distinguish between the present numerical calculations and the pure Coulomb spectrum obtained by neglecting the short-range potential, V_{AA}, between the two heavy A particles. We compare these results in the first two columns of Table I. The pure Born-Oppenheimer Coulomb estimate of the ground state binding energy is 15% larger than the numerically calculated value. On the other hand, the Coulomb estimates give too small binding for all the excited states. They exploit distances outside the Coulomb-like attractive region.

The ground-state deviations were also found in Ref. [22]. They are necessarily due to the approximations in the Born-Oppenheimer procedure, since the accuracy of our numerical computations are fractions of per-mille. The most obvious reason for these differences is the neglect of the nonvanishing term arising from the heavy-heavy kinetic energy operator. The Born-Oppenheimer wave function depends first of all on the fast coordinate, but there is still also a dependence on the slowly varying coordinate r_{AA}. This term is not included in our Born-Oppenheimer calculation, where the inherent two-step quantization procedure in any case is an approximation.

It is illuminating to compare three-body calculations with the hyperspherical adiabatic expansion method, where the hyperradial part of the kinetic energy operator gives rise to an analogous term [14]. Inclusion or not of this term, in the adiabatic expansion with only one adiabatic potential, provides an upper or lower bound on the correct energy [14]. Including more and more of the higher-lying potentials in this method provides a fully converged solution. The Born-Oppenheimer potential is analogous to the one-potential approximation, which over binds in agreement with the bounds of the mentioned hyperspherical adiabatic method. The simplicity of the Born-Oppenheimer results allows qualitative understanding of spectra and structure, which is appealing even though the Faddeev calculations could speak for themselves. In any case the present Born-Oppenheimer approximation suffices for our purpose.

We now include the AA interaction and focus on the results in Fig. 2 where each level for small $\mathcal{A}$ roughly follows the predictions in Eq. (21). However, the calculated ground-state binding energies for both values, $\mathcal{A} = 0.01, 0.02$, are much larger than the pure Coulomb spectrum, see Table I. The strong short-range AA attraction has its largest effect on the lowest-lying levels, that is, more binding by factors of about 3 and 1.5 for ground and first excited states, respectively. The higher-lying excited states shown in Table I and Fig. 2 feel the long-range non-Coulombic Born-Oppenheimer potential and exhibit a less systematic behavior. As $\mathcal{A}$ increases, the bound states move up in energy, the number decreases, and the Coulomb potential supports fewer and fewer bound states.

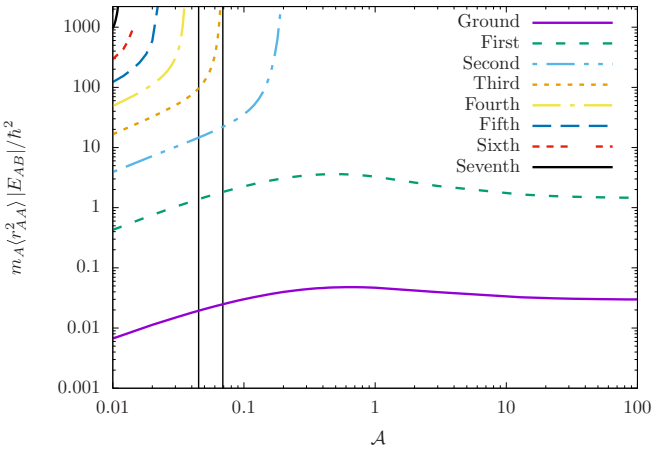

FIG. 3. Dimensionless product $m_A\langle r_{AA}^2\rangle |E_{AB}|/\hbar^2$ ($E_{AA} = E_{AB}$) as a function of the mass ratio $\mathcal{A}$. As $\mathcal{A}$ is increased the radii diverge at the threshold where the excited states disappear. The remaining ground and first excited states assume a constant value as $\mathcal{A} \to \infty$. Vertical lines are the mass ratios corresponding to the systems ^{6}Li-^{133}Cs-^{133}Cs and ^{6}Li-^{87}Rb-^{87}Rb.

B. Sizes

Equipped with an understanding of the energy spectrum as function of the mass ratio we turn to the corresponding underlying structure. We show first in Fig. 3 the calculated mean-square radial distances $\langle r_{AA}^2\rangle$ between the two identical particles. We notice an almost reflected behavior compared to the three-body energies. The radii decrease while the binding energies increase. The two lowest bound states are present for all mass ratios, whereas the sizes for the higher-lying excited states diverge as their energies reach their thresholds for binding.

These radii are for small mass ratios, $\mathcal{A} \ll 1$, related to the Coulombic orbits discussed in connection with Fig. 2. The Coulomb radii are given analytically by

$$\begin{aligned}\langle r_{AA}^2\rangle &= \frac{1}{2}\left(\frac{\hbar^2}{\mu_{AA}Z_{\mathrm{eff}}^2}\right)^2 (n_r+\ell+1)^2 \\ &\quad\times [5(n_r+\ell+1)^2+1-3\ell(\ell+1)] \\ &= \frac{3.1722\hbar^2\mathcal{A}(2n_r+1)^2[5(2n_r+1)^2+7]}{16m_A|E_{AB}|(1+\mathcal{A}/2)},\end{aligned} \tag{22}$$

where we used Eq. (20) and $\ell = -1/2$.

Let us first consider the radii of the states obtained for the smallest mass ratios of $\mathcal{A} = 0.01,\ 0.02$. We compare with the Born-Oppenheimer estimates precisely as we did

TABLE II. Mean-square radii in the Born-Oppenheimer approximation $\langle r_{AA}^{(\mathrm{BO})2}\rangle$, from Eq. (22), and numerical results, respectively, with and without the interaction between the two A particles, $\langle r_{AA}^2\rangle$ and $\langle r_{AA}^{(\mathrm{NI})2}\rangle$. All these lengths are in units of $R_u \equiv \hbar/\sqrt{m_A|E_{AB}|}$.

State	$\mathcal{A}$	$\langle r_{AA}^{(\mathrm{BO})2}\rangle/R_u^2$	$\langle r_{AA}^{(\mathrm{NI})2}\rangle/R_u^2$	$\langle r_{AA}^2\rangle/R_u^2$
Ground	0.01	0.023	0.029	0.006
	0.02	0.047	0.056	0.011
First	0.01	0.923	0.916	0.427
	0.02	1.837	1.767	0.757
Second	0.01	6.510	6.268	3.911
	0.02	12.955	12.254	7.201
Third	0.01	24.359	23.381	16.594
	0.02	48.478	48.534	32.219

for the energies in Table II. As usual for universal structures the radii have the opposite behavior to the energies, that is, the mean-square radii are largest for the smallest binding energies. The Born-Oppenheimer results for the ground state are about 15% smaller than those obtained from the full numerical calculation without an AA interaction. These deviations are again probably mostly due to the neglect of the heavy-heavy kinetic energy operator on the light-particle Born-Oppenheimer wave function. For the excited states the same comparison shows larger Born-Oppenheimer radii. The observed opposite tendencies of energy and radii are reflected in the formulas in Eqs. (21) and (22) where the product is state independent apart from the last factor in Eq. (22).

We now turn to the full calculation with sizable two-body energies between all three pairs of particles, shown in the last column of Table II. The ground-state mean-square radius is a factor of about 3.5 smaller than derived from the Coulomb estimate in Eq. (22). This deviation is again consistent with the similar larger binding energy obtained for that state with the same interaction. The first excited state is only smaller than the Coulomb estimate by a factor of 2.2. The following two higher-lying states have radii rather similar to the Coulomb estimates. These states extend beyond the Coulomb region and into the region of the more confining large-distance Born-Oppenheimer potential from Eq. (19). The effect is a comparably smaller spatial extension which is very close to the results from Eq. (22).

At least one more distance is required to characterize the geometric structure of the three-body system. We first choose the distance r_{AB} between unequal pairs of particles A and B. The mean-square radius is a quantum mechanical expectation value where the two identical particles cannot be distinguished. The results shown in Fig. 4 are therefore averages over distances between particle B and the two A particles. We notice first that the AB mean-square distance is a flat or slightly increasing function with decreasing small mass ratios for both ground and first excited states. The higher-lying states show the opposite tendency of marginal decrease. Furthermore the r_{AB} value in Fig. 4 is much larger than the r_{AA} radius in Fig. 3, although with a difference decreasing with excitation energy. To understand this we cannot turn to the Born-Oppenheimer calculations which only provide information about the AA system while the B coordinate is integrated out. In the limit of small mass

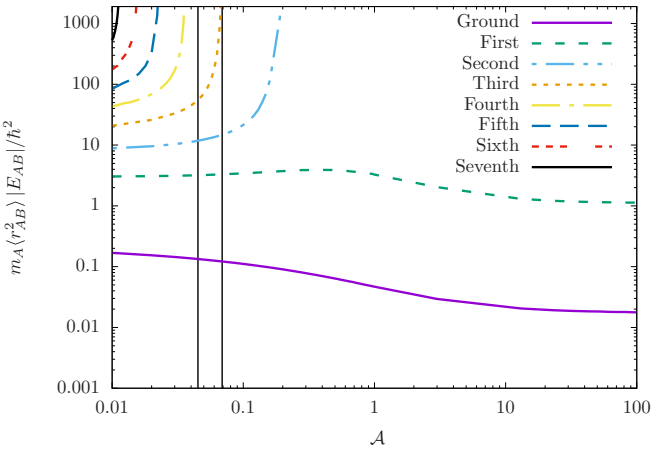

FIG. 4. Same as Fig. 3, but when $\langle r_{AB}^2\rangle$ replaces $\langle r_{AA}^2\rangle$.

ratios the light B particle is very little concerned with the slow relative AA motion. The B particle moves much faster and almost independently in an orbit of much larger radius.

The behavior changes drastically with increasing mass ratios. First the radii of the excited states diverge at their thresholds of binding. Second, the distance r_{AB} decreases with increasing $\mathcal{A}$ for the two bound states. The results for $\mathcal{A} = 1$ agree with the known mean-square ratio of about 70 between the two bound states [14]. As $\mathcal{A}$ increases above 1 we see that the radii only change very little, precisely consistent with the same behavior as shown by the binding energies.

C. Structure

The sizes reflect the structures described by the corresponding wave functions. We would like, schematically and optimistically, to reproduce the relative as well as the absolute sizes in Figs. 3 and 4 by interpretation with appropriate wave functions and/or geometric configurations. We focus on a large mass ratio of $\mathcal{A} = 100$ where the ratio between mean-square distances of AA and AB particles is 1.67 and 1.3 for ground and excited states, respectively. A fully symmetric wave function in hyperspherical coordinates corresponds to $\rho^{-3/2}\exp(-\kappa\rho)$ where ρ in the present case is defined by

$$(2m_A + m_B)\rho^2 = m_A(\vec{r}_A - \vec{r}_{A'})^2 + m_B(\vec{r}_A - \vec{r}_B)^2 + m_B(\vec{r}_{A'} - \vec{r}_B)^2, \tag{23}$$

where the κ value is given by $\hbar^2\kappa^2 = 2m_A|E_3|$. This wave function has the correct large-distance asymptotic behavior. The mean-square radius between a pair of particles, i and k, is then from this very simplified symmetric wave function found by straightforward calculations to give

$$\langle r_{ik}^2\rangle = \hbar^2/(8\mu_{ik}|E_3|), \tag{24}$$

where μ_{ik} is the reduced mass of particles i and k ($i,k = A, A', B$). We shall refer to it as a symmetric estimate since it is obtained from the fully symmetric wave function. This schematic estimate from Eq. (24) for the AA mean-square radii of ground and excited states is smaller by a factor of 2.6 and 8.8, respectively. The corresponding ratios for the AB mean-square radii are 3.1 and 14 which first of all reflect the different

reduced mass dependence. These numbers are for squared radii, and the linear distances, obtained by taking the square root, then only deviate by factors varying from 1.5 to about 4.

Extreme asymmetric structures may be viewed with two particles in a bound state at small distance and the third particle more loosely bound at a larger distance. To produce a finite AA distance the configuration must correspond to a structure like A-(AB) [see Eq. (22)]. The mean-square radius is then $\hbar^2/(4\mu_{A,AB}|E_{A,AB}|)$ which again is inversely proportional to the two-body reduced mass of the distant A particle relative to the stronger bound AB entity. However, the absolute value of this estimate lies between those of ground and excited states for a reasonable choice of $E_{A,AB} \approx 2 \times E_{AB}$.

Both extreme structures of total symmetry and extreme asymmetry fail to reproduce the calculated moments. Furthermore, the large difference between ground and excited states indicate a sizable structure variation. The ground state is within a factor of 2 from the symmetric estimate, whereas the excited state extends in size substantially beyond the inverse three-body energy relation in Eq. (24). The latter is more reminiscent of the huge increase of radii found in the Efimov states which in three dimensions are coherent superpositions of asymmetric geometric structure.

Let us finally consider asymmetric structures where a finite average radius is assumed between the strongest bound AB two-body substructure. We first assume a given distance $r_{AA'}$ between the two A particles, where the B particle moves in a uniform circular orbit of size $r_{A'B}$ around one of the A' particles. Then we estimate the mean-square distance $\langle r^2_{AB}\rangle \approx (\langle r^2_{AA'}\rangle + \langle r^2_{A'B}\rangle)/2$, where $1/2$ is from adding the two symmetrized configurations. To reproduce the calculated mean-square radii we need $\langle r^2_{AB}\rangle/\langle r^2_{AA}\rangle \approx 0.2{,}0.5$ for ground and excited states. These values show a strong tendency toward symmetric configurations.

The sizes are often measured as distances relative to the total center of mass. This only provides little additional information but it is very illustrative besides serving as a consistency check on our understanding of the underlying structures. We show in Fig. 5 the mean-square radial distance of particles A from

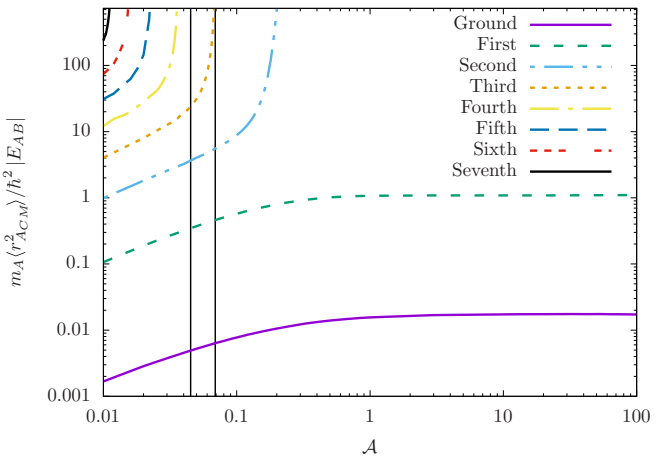

FIG. 5. Same as Fig. 3, but when the mean-square distance $\langle r^2_{A_{C.M.}}\rangle$ from C.M. to particle A replaces $\langle r^2_{AA}\rangle$, as $\mathcal{A} \to \infty$ $\langle r^2_{A_{C.M.}}\rangle \to \langle r^2_{AB}\rangle$.

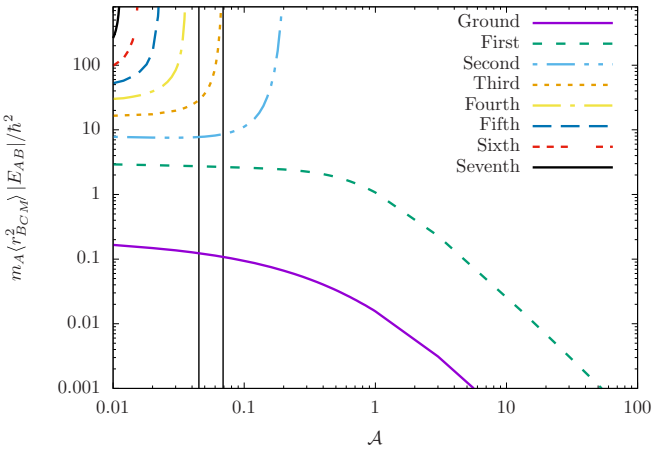

FIG. 6. Same as Fig. 5, but when the mean-square distance $\langle r^2_{B_{C.M.}}\rangle$ from C.M. to particle B replaces $\langle r^2_{A_{C.M.}}\rangle$, as $\mathcal{A} \to \infty$ $\langle r^2_{B_{C.M.}}\rangle \to 0$.

the center of mass. The two limits of $\mathcal{A}$ differ very much from each other. Varying $\mathcal{A}$ from small to large values causes the three-body center of mass to move from the center of mass of the AA system to the center of particle B. This implies by geometric reasoning that $\sqrt{\langle r^2_A\rangle}$ approaches $\sqrt{\langle r^2_{AA}\rangle}/2$ and $\sqrt{\langle r^2_{AB}\rangle}$ in these two limits, respectively. These predictions are confirmed by comparing Fig. 5 with the results in Figs. 3 and 4, that is, observing that $\langle r^2_A\rangle \to \langle r^2_{AA}\rangle/4$ and $\langle r^2_A\rangle \to \langle r^2_{AB}\rangle$ for small and large $\mathcal{A}$.

The different behavior of $\langle r^2_B\rangle$ is seen in Fig. 6. The geometry now predicts that r_B should vanish for large $\mathcal{A}$ since the total center of mass coincides with the center of particle B. In the other limit of small $\mathcal{A}$ we know that $\langle r^2_{AA}\rangle \ll \langle r^2_{AB}\rangle$ and consequently $\langle r^2_B\rangle$ should approach $\langle r^2_{AB}\rangle$, since the AA system looks like an entity from far away where particle B is located. Again these predictions are confirmed numerically by comparing Figs. 4 and 6.

There is a lack of experimental information concerning the sizes of these systems in two dimensions. However, we are able to compare our results for $\mathcal{A} = 1$ with those from Ref. [14] as follows. The spatial extension of a system can be measured by radial moments. Often the second moment, the root-mean-square radius, is used as an average measure. Different distributions can be of interest as exemplified by average charge or mass radii. For a self-supported system of bound particles the center of mass is conserved and it is natural to measure all distances with respect to this point, $\vec{R}_{\rm C.M.}$. The corresponding expectation value is related to the root-mean-square radius $R_{\rm rms}$ of the mass distribution as defined for our three-body system by

$$R^2_{\rm rms}\sum_{k=A,A',B} m_k = \sum_{k=A,A',B} m_k\langle(\vec{r}_k - \vec{R}_{\rm C.M.})^2\rangle = \sum_{k=A,A',B} m_k\langle\vec{r}^{\,2}_{k_{\rm C.M.}}\rangle, \tag{25}$$

where the vectors $\vec{r}_{k_{\rm C.M.}}$ by definition connect particle k and the center of mass of the three-body system. The three-body center of mass lies on the line connecting particle A with the center of

mass of the remaining pair of AB particles, and analogously for particle B. We therefore have the relations

$$\langle r^2_{A_{\text{C.M.}}}\rangle = \left(\frac{1+\mathcal{A}}{2+\mathcal{A}}\right)^2 \langle r^2_A\rangle, \tag{26}$$

$$\langle r^2_{B_{\text{C.M.}}}\rangle = \left(\frac{2}{2+\mathcal{A}}\right)^2 \langle r^2_B\rangle, \tag{27}$$

which can be used to express R^2_{rms} from Eq. (25) in terms of different mean-square radii, that is,

$$\begin{aligned} R^2_{\text{rms}} &= \frac{2\langle r^2_{A_{\text{C.M.}}}\rangle + \mathcal{A}\langle r^2_{B_{\text{C.M.}}}\rangle}{2+\mathcal{A}} \\ &= 2\frac{(1+\mathcal{A})^2}{(2+\mathcal{A})^3}\langle r^2_A\rangle + \frac{4\mathcal{A}}{(2+\mathcal{A})^3}\langle r^2_B\rangle. \end{aligned} \tag{28}$$

For three identical particles, where $\mathcal{A}=1$ and $\langle r^2_A\rangle = \langle r^2_B\rangle$, this relation reduces to

$$R_{\text{rms}} = \tfrac{2}{3}\sqrt{\langle r^2_A\rangle}, \tag{29}$$

with $\langle r^2_A\rangle$ plotted in Fig. 5.

The two bound three-body states labeled 0 and 1 are in [14] found to have root-mean-square radii given by

$$R^{(0)}_{\text{rms}} = 0.111a = 0.125\sqrt{\frac{\hbar^2}{m_A|E_{AB}|}}, \tag{30}$$

$$R^{(1)}_{\text{rms}} = 0.927a = 1.041\sqrt{\frac{\hbar^2}{m_A|E_{AB}|}}, \tag{31}$$

where the two-dimensional scattering length a is related to the two-body energy $E_{AA} = E_{AB} = -4e^{-2\gamma}\hbar^2/(m_A a^2)$. These values match exactly our numerical results.

D. Threshold behavior

We want now to investigate in more detail how the structure varies with mass ratio when the energy of a state approaches its threshold for binding. We know that in three dimensions the sizes of bosonic three-body systems diverge logarithmically at their three-body energy thresholds. In contrast, the sizes remain finite for Brunnian systems (all pairs are unbound) with more than three bosons [31], even at their corresponding thresholds of binding. In these cases, the thresholds are reached from the bound side by decreasing the two-body attraction. In the present study we are decreasing the mass ratio and in practice decreasing the effective interaction between the constituents of the system.

Again we use the mean-square radii as indicative measures. We focus on the second excited state which is the lowest-lying state with diverging size. Its behavior is repeated by the other excited states, which we therefore do not need to discuss in this paper. We show in Fig. 7 the results as functions of $\mathcal{A}$ for the different radii of the second excited state. We multiply the radii by the energy deviation from the two-body threshold, $|E_3 - E_{AB}|$, in order to extract the behavior of the divergence. The striking result is that this product converges toward a constant as the threshold is approached. Thus, the divergence of the mean-square radius is inversely proportional

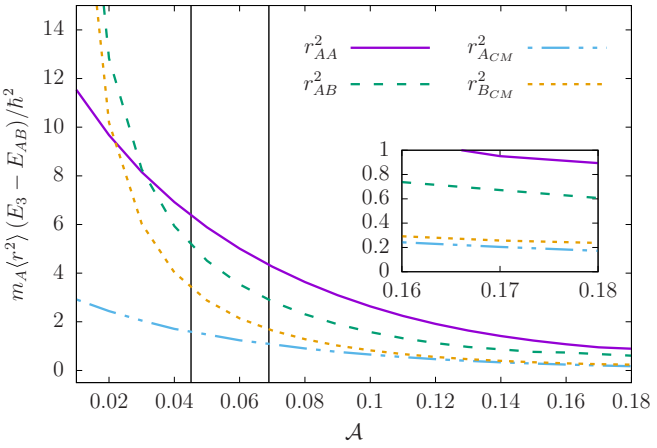

FIG. 7. Threshold behavior of different mean-square radii for the second excited state as a function of mass ratio. The divergent mean-square radii multiplied by $E_3 - E_{AB}$ reach constant values at threshold. Vertical lines are the mass ratios corresponding to the systems ^{6}Li-^{133}Cs-^{133}Cs and ^{6}Li-^{87}Rb-^{87}Rb.

to $E_3 - E_{AB}$. This behavior is well-known for weakly bound two-body halos in three dimensions [6] and shown in Ref. [14] to be valid also in two dimensions. The implication is that the threshold structure must correspond to one particle moving away from a bound and spatially confined subsystem, which in our case only can be a bound dimer.

Two structures are possible at threshold, that is, either particle A or particle B is ejected while the remaining pair settles in their ground state. In both cases the threshold structure resembles two-body systems, that is, (AA)-B or (AB)-A with corresponding reduced masses $\mu_{AA,B} \approx 0.18$ or $\mu_{AB,A} \approx 0.54$, where the numbers are obtained with a threshold value of $\mathcal{A} \approx 0.2$.

These structures would according to Ref. [14] lead to the two-body divergence, $\langle r^2_{ik}\rangle = \hbar^2/(3\mu_{ik}|E_{\text{th}}|)$, where μ_{ik} and $|E_{\text{th}}|$ are two-body reduced mass and the vanishing threshold energy, respectively. This means that the curves in Fig. 7 for $m_A\langle r^2_{ik}\rangle|E_{\text{th}}|/\hbar^2 = m_A/(3\mu_{ik})$ can be either 1.85 or 0.62. Thus, $(m_A\langle r^2_{AA}\rangle|E_{\text{th}}|/\hbar^2, m_A\langle r^2_{AB}\rangle|E_{\text{th}}|/\hbar^2) \to (0.0, 1.85)$ or $(m_A\langle r^2_{AA}\rangle|E_{\text{th}}|/\hbar^2, m_A\langle r^2_{AB}\rangle|E_{\text{th}}|/\hbar^2) \to (0.62, 0.62)$ are the two corresponding two-body threshold structures, where either B or A are ejected. The two identical finite values in the latter case are due to the same distance between the ejected A particle and both the remaining A and B particles in a bound state.

Obviously the best match to the results displayed in Fig. 7 is ejection of one of the A particles. In the calculated expectation value is contained an average over the distances between the two A particles and particle B. One of these distances remains finite and does not contribute except through a reduction of the probability by a factor of 2. This accounts for the value of $\frac{m_A\langle r^2_{AB}\rangle}{\hbar^2}(E_3 - E_{AB}) = 0.6$, being only about two thirds of $\frac{m_A\langle r^2_{AA}\rangle}{\hbar^2}(E_3 - E_{AB}) = 0.9$, at threshold.

IV. SUMMARY, CONCLUSIONS, AND PERSPECTIVES

We studied the structures of three-body systems in two spatial dimensions. We concentrate on asymmetric systems

formed by two identical bosons and a third particle. We assume spin-independent interactions and all results are therefore also valid for two identical fermions with spatially symmetric wave functions. We use two-body zero-range interactions and the Faddeev equations in momentum space to solve the three-body problem. Universal properties are then emphasized due to the vanishing interaction range. The three-body system is characterized by two masses and two zero-range strength parameters chosen to reproduce specified two-body energies. The equations only depend on two parameters, that is, mass and energy ratios. In this paper we essentially only investigate the mass dependence for equal two-body energies.

Our aim is to obtain information about universal structures. We calculate second-order radial moments corresponding to two independent distances within the three-body system. Correlations between these quantities are very indicative of the underlying dominating structure. Relatively low orders of radial moments are substantially easier to compute than the density distributions, especially when the starting point is in momentum space. We therefore first derive suitable expressions for the desired radial moments expressed in terms of single first-order derivatives of integrals over momentum-space wave functions.

We first calculate and analyze the energy spectrum as the primary characterizing quantity of any quantum system. We keep equal two-body energies. The number of bound states are always finite but varies from 2 and upward, diverging as the relative mass of the distinguishable particle decreases from very large to approaching zero. Only precisely two bound states are present as for equal masses until the mass ratio has decreased to about 0.2. Then a third state appears followed by numerous other states as the mass ratio decreases toward zero. This agrees qualitatively with similar previous observations, as well as quantitatively for the known case of equal masses.

We analyze the spectra for small mass ratio by use of the Born-Oppenheimer approximation of the potential. The effective interaction generated by the light particle has Coulomb behavior for small distances between particles of the heavier pair. Combining with the kinetic energy operator in two dimensions the Coulomb energy spectrum appears for an angular momentum quantum number equal to $-1/2$. The small-distance region is the most attractive region, where the short-range interaction between the two heavy particles also is strongest. Consequently this is where the lowest states are located.

Considering this Coulomb potential calculated for small mass ratios from the Born-Oppenheimer approximation, the three-body energies and heavy-heavy mean-square radii are derived and compared to the full calculations. We see that the numerically obtained ground state is more bound with a smaller radius than arising from the Coulomb estimate. This is due to the additional attractive heavy-heavy zero-range interaction. The first few of the following higher-lying states still feel the heavy-heavy short-range interaction but they have energies and radii closer to the Coulomb estimates. This reflects that the effect of the zero-range attraction quickly decreases as the states move to larger distances. The higher-lying excited states extend spatially beyond the Coulomb-like potential, but all bound states are eventually confined within the exponentially decaying Born-Oppenheimer potential at large distance.

The mean-square radii are to a large degree a reflection of the energies, that is, small energy corresponds to a large radius and vice versa. This is the general observation for universal properties when all angular momenta are zero or vanishingly small. By comparing two independent lengths in the same three-body system we can generate a geometric picture of an underlying schematic structure. The variation with mass ratio is substantial. The two remaining states for moderate and large mass ratios appear to be consistent with the light particles at roughly twice the distance between light and heavy particles. For small mass ratios we find for both ground and excited states that the light particle is located at distances much larger than the distance between the two heavy particles.

The disappearance of excited states into the continuum for threshold values of the mass ratio is related to specific bound-state structures close to the thresholds. The mean-square radii here prove themselves to be efficient measures of the corresponding structures. We show numerically that these mean-square radii diverge inversely proportional to the deviation of the three-body energy from the two-body threshold energy. Comparing distances between identical and unequal particles we conclude that the threshold structure corresponds to one of the identical particles far away from a bound dimer of the other two particles. Thus, this far-away particle is being ejected into the continuum. It should be possible to confirm these predictions by cold atom experiments where three-body atomic systems of ^{6}Li-^{133}Cs-^{133}Cs and ^{6}Li-^{87}Rb-^{87}Rb, among others, are already produced in laboratories.

The technique we developed is based on the schematic, but hugely popular, zero-range interaction treated in momentum space. This interaction is the extreme limit of a short-range potential, and therefore in general the simplest tool to provide quantitative information about universal properties. The present method to calculate mean-square radii is a special application to derive structure information through expectation values. The method is simpler and faster than using brute force to obtain wave functions which afterward supply the desired observables. An interesting continuation of the present study is to extend it to more than three atoms and see how the universal relations derived in [29] would change for a mass-imbalanced system.

The method can be used directly to investigate the dependence of radii on the strengths of the two-body interactions. The formalism can be relatively easily generalized to apply to three-body systems where one or more two-body subsystems are unbound, whereas the three-body system still remains bound. All applications may be extended to three distinguishable particles with their different masses and interaction parameters. The application to two spatial dimensions is interesting because this is a rigorous limit with unique properties compared to other geometries. However, both one and three dimensions are equally accessible, and a continuous variation between dimensions also becomes increasingly interesting.

ACKNOWLEDGMENT

This work was partly supported by funds provided by the Brazilian agencies FAPESP (2016/01816-2), CNPq, and CAPES (88881.030363/2013-01).

[1] C. J. Pethick and H. Smith, *Bose-Einstein Condensation in Dilute Gases* (Cambridge University Press, New York, 2008), Chap. 5.
[2] G. Modugno, F. Ferlaino, R. Heidemann, G. Roati, and M. Inguscio, Phys. Rev. A **68**, 011601 (2003).
[3] K. Günter, T. Stöferle, H. Moritz, M. Köhl, and T. Esslinger, Phys. Rev. Lett. **95**, 230401 (2005).
[4] F. Werner and Y. Castin, Phys. Rev. A **86**, 053633 (2012).
[5] F. F. Bellotti and M. T. Yamashita, Few-Body Syst. **56**, 905 (2015).
[6] A. S. Jensen, K. Riisager, D. V. Fedorov, and E. Garrido, Rev. Mod. Phys. **76**, 215 (2004).
[7] E. Braaten and H. W. Hammer, Phys. Rep. **428**, 259 (2006).
[8] T. Frederico, L. Tomio, A. Delfino, M. R. Hadizadeh, and M. T. Yamashita, Few-Body Syst. **51**, 87 (2011).
[9] M. Kunitski *et al.*, Science **348**, 551 (2015).
[10] W. Cencek *et al.*, J. Chem. Phys. **136**, 224303 (2012).
[11] E. A. Kolganova, A. K. Motovilov, and W. Sandhas, Few-Body Syst. **51**, 249 (2011).
[12] G. V. Skornyakov and K. A. Ter-Martirosyan, Sov. Phys. JETP **4**, 648 (1957).
[13] V. Efimov, Phys. Lett. B **33**, 563 (1970); Nucl. Phys. A **362**, 45 (1981).
[14] E. Nielsen, D. V. Fedorov, A. S. Jensen, and E. Garrido, Phys. Rep. **347**, 373 (2001).
[15] M. T. Yamashita, F. F. Bellotti, T. Frederico, D. V. Fedorov, A. S. Jensen, and N. T. Zinner, J. Phys. B **48**, 025302 (2015).
[16] L. W. Bruch and J. A. Tjon, Phys. Rev. A **19**, 425 (1979).
[17] S. K. Adhikari, Am. J. Phys. **54**, 362 (1986).
[18] S. K. Adhikari, A. Delfino, T. Frederico, and L. Tomio, Phys. Rev. A **47**, 1093 (1993).
[19] E. Nielsen, D. V. Fedorov, and A. S. Jensen, Few-Body Syst. **27**, 15 (1999).
[20] F. F. Bellotti, T. Frederico, M. T. Yamashita, D. V. Fedorov, A. S. Jensen, and N. T. Zinner, J. Phys. B **44**, 205302 (2011).
[21] F. F. Bellotti, T. Frederico, M. T. Yamashita, D. V. Fedorov, A. S. Jensen, and N. T. Zinner, Phys. Rev. A **85**, 025601 (2012).
[22] F. F. Bellotti, T. Frederico, M. T. Yamashita, D. V. Fedorov, A. S. Jensen, and N. T. Zinner, J. Phys. B **46**, 055301 (2013).
[23] N. N. Khuri, A. Martin, and T.-T. Wu, Few-Body Syst. **31**, 83 (2002).
[24] J. Levinsen, P. Massignan, and M. M. Parish, Phys. Rev. X **4**, 031020 (2014).
[25] J. P. D'Incao and B. D. Esry, Phys. Rev. A **90**, 042707 (2014).
[26] J. P. D'Incao, F. Anis, and B. D. Esry, Phys. Rev. A **91**, 062710 (2015).
[27] T. K. Lim and B. Shimer, Z. Phys. A **297**, 185 (1980).
[28] M. T. Yamashita, R. S. Marques de Carvalho, L. Tomio, and T. Frederico, Phys. Rev. A **68**, 012506 (2003).
[29] H.-W. Hammer and D. T. Son, Phys. Rev. Lett. **93**, 250408 (2004).
[30] A. C. Fonseca, E. F. Redish, and P. E. Shanley, Nucl. Phys. A **320**, 273 (1979).
[31] M. T. Yamashita, D. V. Fedorov, and A. S. Jensen, Phys. Rev. A **81**, 063607 (2010).